Change in Crystal Orientation of a {100}<001> Pure Aluminum Single Crystal during Accumulative Roll Bonding

AUTHOR(S):

Kashihara, K.; Ikushima, W.; Miyajima, Y.; Terada, D.; Tsuji, N.

CITATION:

Kashihara, K. ...[et al]. Change in Crystal Orientation of a {100}<001> Pure Aluminum Single Crystal during Accumulative Roll Bonding. Materials transactions 2011, 52(5): 825-829

ISSUE DATE:

2011-04

URL:

http://hdl.handle.net/2433/171916

Materials Transactions, Vol. 52, No. 5 (2011) pp. 825 to 829
Special Issue on Aluminium Alloys 2010

Change in Crystal Orientations of a {100} ⟨001⟩ Pure Aluminum Single Crystal during Accumulative Roll Bonding*

K. Kashihara[1], W. Ikushima[1], Y. Miyajima[2], D. Terada[2] and N. Tsuji[2]

[1]*Wakayama National College of Technology, Gobo 644-0023, Japan*
[2]*Kyoto University, Kyoto 606-8501, Japan*

A {100} ⟨001⟩ pure aluminum single crystal specimen was deformed by accumulative roll bonding (ARB) up to 9 cycles ($\varepsilon_{eq} = 7.18$) with lubrication. The 5- and 9-cycle processes developed weakened textures composed of {123} ⟨634⟩ and {112} ⟨111⟩. The {100} ⟨001⟩ areas existed even after the 9th cycle. The area fraction of {100} ⟨001⟩ was almost the same as that of the 2-cycle processed specimen. The average area fraction of {100} ⟨001⟩ was 4.8%. The cross slips by primary slip pairs may play an important role in maintaining the {100} ⟨001⟩ area. In the 5-cycle processed specimen, {123} ⟨634⟩ bands were observed in not only the center layer but also the one-eighth thickness layers close to the specimen surfaces. After the 7th and 9th cycles, {112} ⟨111⟩ was observed to form by further crystal rotation from {123} ⟨634⟩.
[doi:10.2320/matertrans.L-MZ201109]

(Received September 27, 2010; Accepted February 3, 2011; Published April 13, 2011)

Keywords: *sever plastic deformation, aluminum, single crystal, rolling, local texture*

1. Introduction

Ultra grain refinement is achieved by severe plastic deformation techniques such as HTP (High Pressure Torsion),[1–3] ECAP (Equal-Channel Angular Pressing),[1,4] CEC (Cyclic Extrusion and Compression),[5,6] and ARB.[7,8] Among these processes, ARB has the advantage that it can be used to produce large bulky materials. The development of microstructures[9–11] and the characteristic of mechanical properties using the ARB process have been studied.[12,13] Ultra fine grain structures are generally considered to form by accumulation of abundant strain imposed into the material.[14,15]

In FCC metals such as aluminum, the crystal orientation {100} ⟨001⟩ is of great interest in texture control.[16] When a heavy cold-rolled aluminum specimen is annealed under certain heat treatment conditions, the recrystallization texture contains a main {100} ⟨001⟩ component. One of the origins of {100} ⟨001⟩ recrystallization nuclei is considered to be the {100} ⟨001⟩ band existing in the deformed structure, called "the cube band", which is arrayed between deformation regions with major rolling texture components such as {123} ⟨634⟩ and {112} ⟨111⟩.[17] It was clarified that the stability of {100} ⟨001⟩ area during rolling was enhanced by the constraint of grain boundaries,[18] and the preferred nucleation of {100} ⟨001⟩ recrystallized grain was dependent on both orientation gradient and stored energy.[19]

One of the present authors investigated the evolution of texture and microstructure in cold-rolled {100} ⟨001⟩ aluminum single crystals.[20,21] When the thickness was reduced by more than 50%, a banded structure consisting of two matrices was observed on a mid-thickness plane parallel to the rolling plane. The transition bands between the matrices corresponded to the cube bands. It was empirically demonstrated that the banded structure easily develops when the initial orientation of the single crystal deviates by 5° from the ideal {100} ⟨001⟩ orientation. We have further interest in the stability of cube bands during severe plastic deformation more than 99% thickness reduction.

In the former paper, {100} ⟨001⟩ aluminum single crystals were heavily deformed using ARB to clarify whether {100} ⟨001⟩ deformed areas can survive upon severe plastic deformation. The change in rolling texture components was also clarified.[22] In this paper, further results were added, and deeper discussions were carried out, especially in order to discuss the distribution of deformed areas with β-fiber texture components and {100} ⟨001⟩ through the specimen thickness.

2. Experimental Procedure

A {100} ⟨001⟩ single crystal plate was made from a 99.99% aluminum ingot using the modified Bridgeman method. Specimens for rolling had dimensions of 60 mm × 16 mm × 4 mm; they were cut from the plate by an electric discharge machine. The surfaces of the specimens were mechanically and electrolytically polished.

The single crystal specimens had an initial orientation that deviated by 1.5° from the ideal {100} ⟨001⟩. A schematic illustration depicting primary slip systems on eight {111} slip planes is shown in Fig. 1. The designation for slip systems follows the notation proposed by Bishop and Hill,[23] where alphabets a-d and numbers 1-6 indicates {111} slip planes and ⟨110⟩ slip directions, respectively. Assuming that a single crystal during rolling is deformed in compression along the normal direction (*ND*) and in tension along the rolling direction (*RD*), slip system pairs of a2–d2 and b2–c2 become the primary slip systems. Here, these slip system pairs have a cross-slip relationship to each other.

During the ARB process, the single crystal specimens were deformed by a two-high rolling mill with rolls of 310 mm diameter at room temperature with lubrication. The principle of the ARB process has previously been described in detail.[7] The thickness reduction per cycle was 50% except for the

*The Paper Contains Partial Overlap with the ICAA12 Proceedings by USB under the Permission of the Editorial Committee.

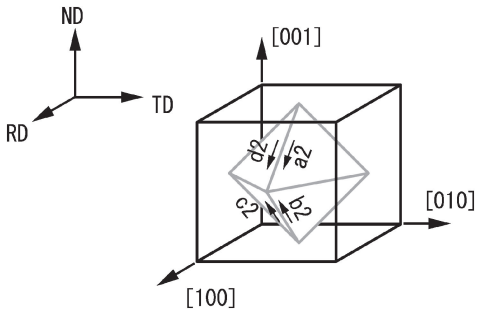

Fig. 1 Schematic illustration depicting primary slip systems on eight {111} slip planes.

Table 1 The thickness reduction, equivalent strain and total thickness of specimen in each cycle. At the 1st and 2nd cycles, conventional rolling was conducted. Roll-bonding was carried out after the 3rd cycle.

Cycle	1	2	3	4	5	7	9
Thickness reduction	0.5	0.75	0.875	0.9375	0.9688	0.9922	0.998
Equivalent strain	0.8	1.6	2.4	3.2	4	5.6	7.18
Total thickness (mm)	2	1	1	1	1	1	1

1st cycle, where the 4 mm thick specimen was rolled down to 2 mm in two passes. The 1st and 2nd cycles did not use roll-bonding but conventional rolling. Cutting, stacking and roll-bonding were conducted after the 3rd cycle. Just after roll-bonding, the rolled specimen was immediately cooled into water. By repeating the ARB process, the 9-cycle processed specimen was obtained. Table 1 shows the thickness reduction and equivalent strain during the ARB process. The thickness reduction and equivalent strain imposed on a specimen after the 9th cycle were $r = 99.8\%$ and $\varepsilon_{eq} = 7.18$, respectively.

The crystal orientations through the thickness of the processed specimens were measured by a field emission type scanning electron microscope (FEI XL30S) equipped with an EBSD system. The observation plane was normal to the transverse direction (*TD* plane). The scan step for crystal orientation measurement was carried out at 1 µm. In the 9-cycle processed specimen, the crystal orientations were measured at 0.5 µm steps for more precise orientation analysis. The crystal orientations were analyzed by commercial software (TSL-OIM analysis). The high angle boundary was defined as that having misorientation larger than 15°. Crystal orientations of {100} ⟨001⟩, {102} ⟨201⟩, and {100} ⟨011⟩ that had a tolerance within 15° from the ideal orientation were represented as the crystal orientation components. In this study, the tolerance value for classifying the crystal orientations was 10° for {110} ⟨112⟩, {123} ⟨634⟩, and {112} ⟨111⟩ to avoid overlapping representation of crystal orientations.

3. Experimental Results

Figure 2 shows the {111} pole figures constructed from the EBSD data of the 1-, 5-, and 9-cycle processed specimens. These textures reveal the crystal orientations viewed from the *ND* plane. In 1-cycle processed specimens, the main orientation rotated about the *TD* with respect to the initial orientation. The 5- and 9-cycle processes developed weakened textures composed of {123} ⟨634⟩ and {112} ⟨111⟩. In the 9th cycle pole figure, crystal rotation about *TD* axis was observed relative to the texture components of the 5-cycle processed specimen.

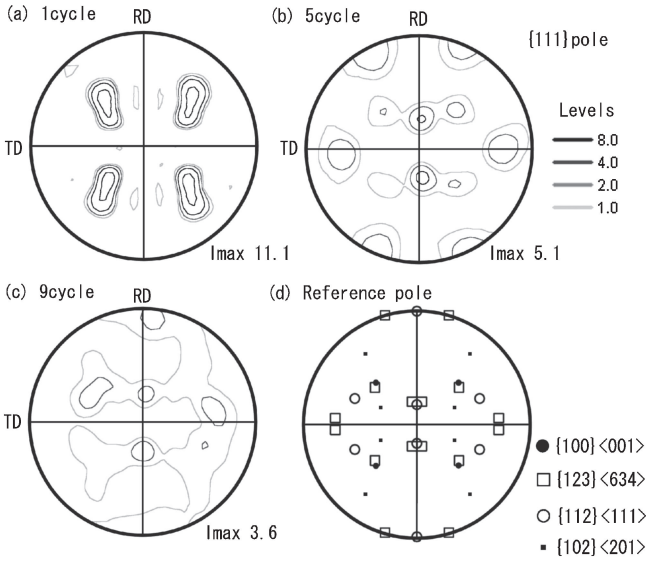

Fig. 2 {111} pole figures of the 1-, 5-, and 9-cycle processed specimens.

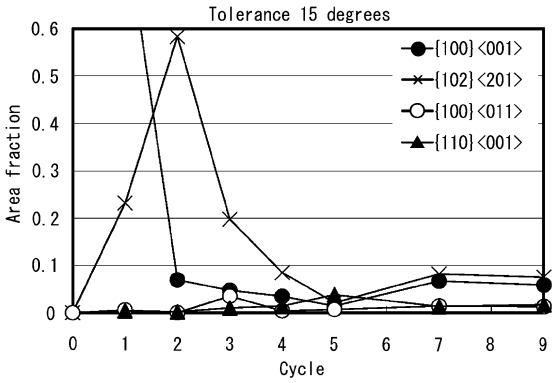

Fig. 3 Change in area fractions of {100} ⟨001⟩, {102} ⟨201⟩, {100} ⟨011⟩ and {110} ⟨011⟩ with increasing the number of cycles. The tolerance value for classifying the crystal orientation was 15°.

Figure 3 shows the change in area fractions of {100} ⟨001⟩, {102} ⟨201⟩, {100} ⟨011⟩ and {110} ⟨001⟩ with increasing the number of ARB cycles. The tolerance value used for classifying the crystal orientation was 15°. The area fraction of {100} ⟨001⟩ was 82.3% after the 1st cycle. It abruptly decreased to 6.9% after the 2nd cycle. Furthermore, the ARB cycles produced little significant change in the area fraction of {100} ⟨001⟩. After the 9th cycle the area fraction of {100} ⟨001⟩ was 5.8%. The area fraction of {102} ⟨201⟩ reached its maximum in the specimen after the 2nd cycle and decreased with further ARB processing. The {100} ⟨011⟩ and {110} ⟨001⟩ orientations did not develop in the {100} ⟨001⟩ aluminum single crystal deformed by the ARB process under lubricated conditions.

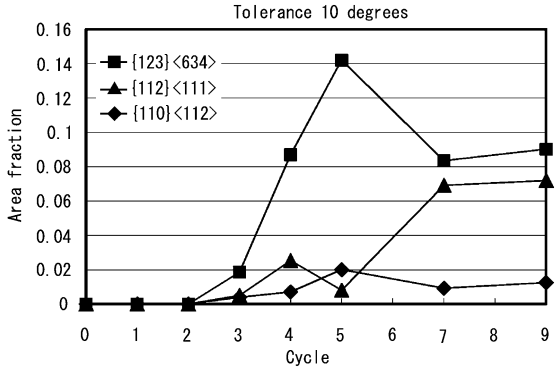

Fig. 4 Change in area fractions of {110} ⟨112⟩, {123} ⟨634⟩, and {112} ⟨111⟩ with increasing the number of cycles. The tolerance value for classifying the crystal orientation was 10°.

Figure 4 shows the area fractions of {110} ⟨112⟩, {123} ⟨634⟩, and {112} ⟨111⟩ within 10° from the ideal orientations. These crystal orientations are typical texture components in rolled FCC metals, which could be distinguished after the 3rd cycle. In the 5-cycle processed specimen, {123} ⟨634⟩ had the maximum area fraction of 14.2%. The area fraction of {112} ⟨111⟩ increased up to 6.9% after the 7th cycle, while the area fraction of {123} ⟨634⟩ was reduced to 8.3%. The area fraction of {112} ⟨111⟩ in the 9-cycle processed specimen was 7.2%, which was second next to that of {123} ⟨634⟩.

Figure 5 shows a crystal orientation map for each processed specimen. This map depicts {100} ⟨001⟩, {102} ⟨201⟩, and {100} ⟨011⟩ within 15° from the ideal orientations and {110} ⟨112⟩, {123} ⟨634⟩, and {112} ⟨111⟩ within 10°. In the 2-cycle processed specimen, the matrix bands of M1 and M4 had {102} ⟨201⟩, which were obtained by crystal rotation about the *TD* axis with respect to the initial orientation. The macroscopic subdivision of the single crystal and the crystal orientations in four matrix bands were described in detail in the former paper.[22] The transition bands between the four matrix bands were colored by red, indicating {100} ⟨001⟩. The 3-cycle process developed thick and thin bands consisting of {100} ⟨001⟩ and {102} ⟨201⟩. The {123} ⟨634⟩ areas started to form after the 3rd cycle. The {123} ⟨634⟩ bands became thinner with increasing the number of ARB cycles, and the number of the bands increased. In the 5-cycle processed specimen, the {123} ⟨634⟩ bands were observed in one-eighth thickness layers close to the specimen surfaces.

Figure 6 shows a magnified deformation structure in the 9-cycle processed specimen. The lamellar band structure parallel to the *RD* was composed of {100} ⟨001⟩, {102} ⟨201⟩, {123} ⟨634⟩, and {112} ⟨111⟩.

The mean grain size along the *ND* in the 5-, 7- and 9-cycle processed specimens had sizes of 1.60, 1.42, and 0.88 μm, respectively. The grain sizes after 5 and 7 cycles were smaller than a mean grain size of 1.80 μm after the 6th cycle with lubrication in {110} ⟨112⟩ pure aluminum single crystals.[24] In ARB experiments using pure aluminum polycrystal, it was reported that mean grain sizes after the 8th ARB cycle ($\varepsilon_{eq} = 6.4$) were about 0.25 μm.[10,14,15] The mean grain size in the single crystal specimens was larger than that in the polycrystal specimens. The difference in grain size could be ascribed to the effect of grain boundaries which exist in polycrystalline material before rolling.

4. Discussion

Ishida *et al.* conducted an ARB experiment using a {112} ⟨110⟩ aluminum single crystal[24] and clarified the macroscopic grain subdivision. The present study especially focuses on the change in rolling texture component developed by the ARB process.

It has been previously reported that a weak rolling texture was developed by the ARB process, nevertheless the material was highly strained.[7] As shown in Fig. 2, the rolling texture obtained by using the single crystals also showed weak rolling textures. The 5- and 9-cycle processed specimens contained {123} ⟨634⟩ and {112} ⟨111⟩, which are typical rolling texture components in rolled FCC metals.

An ARB experiment was carried out by Kamikawa *et al.* using 99.99% pure aluminum polycrystal deformed by ARB for up to 6 cycles without lubrication.[25,26] The grain size along the *ND*, misorientation of grain boundary, and change in crystal orientation were analyzed on the *TD* plane by the EBSD method. The local textures between the surface and inner layers were quite different. The inner layer had local textures consisting of {110} ⟨112⟩, {123} ⟨634⟩, and {112} ⟨111⟩, which were termed "rolling texture components". In this study, it is called "β-fiber texture components". In contrast, the surface layers which had the quarter-thickness of specimen showed the local textures of {100} ⟨011⟩, {111} ⟨112⟩, and {111} ⟨011⟩, called "shear texture components". The crystal orientation distribution through the specimen thickness did not correspond with the accumulation of strain imposed by ARB processes over the 1st to 6th cycles. Kamikawa *et al.* produced a 7-cycle ARB processed specimen and compared the distribution of the crystal orientation through the specimen thickness with that of the 6-cycle processed specimen. The shear texture components observed in the quarter-thickness layers close to the surfaces of the 6-cycle ARB processed specimen were destroyed and rotated into the β-fiber texture components in the inner layer after the 7th ARB cycle. Conversely, the β-fiber texture components observed in the inner layer of the 6-cycle ARB processed specimen were rotated into the shear texture components in the quarter-thickness layers of the 7-cycle ARB processed specimen. This result indicates that the local textures formed through the specimen thickness were easily destroyed by the next ARB process. According to their conclusion, under the unlubricated condition the changes in local textures after every ARB cycle may reduce the intensity of the rolling texture and create the characteristic local texture through the specimen thickness.

As shown in Fig. 4, {123} ⟨634⟩ began to form in the 3-cycle processed specimen. The maximum area fraction was observed in the 5-cycle processed specimen. Figure 5 shows that {123} ⟨634⟩ bands were distributed through the specimen thickness except for regions close to the specimen surfaces. The distribution of {123} ⟨634⟩ observed in this study substantiates the destruction and rotation mechanism of local textures in every ARB cycle proposed by Kamikawa

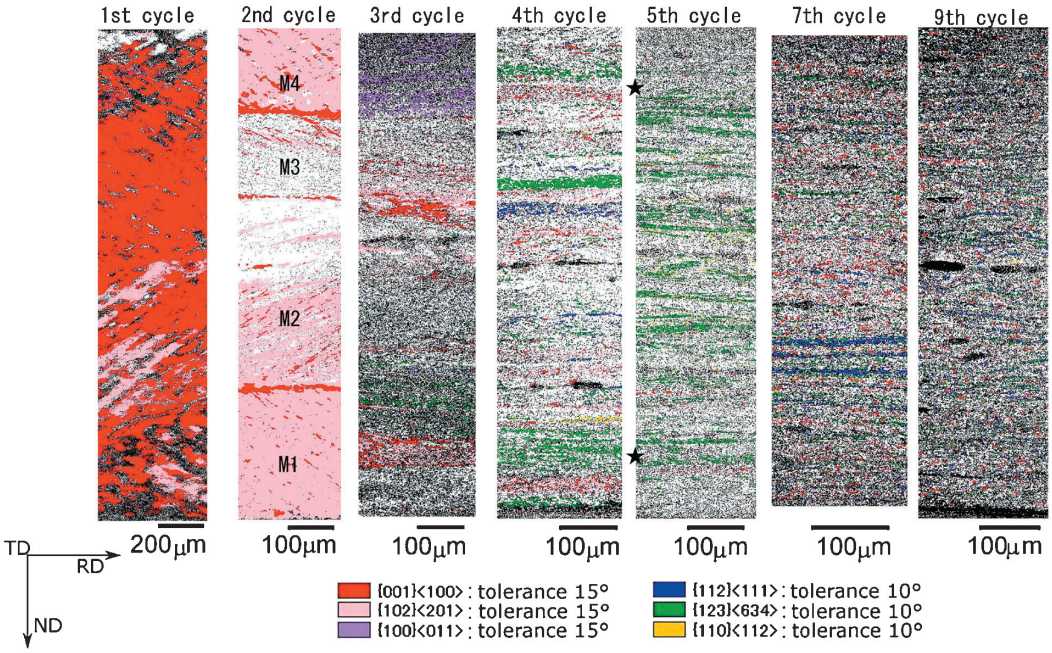

Fig. 5 Crystal orientation maps in processed specimens. These maps show {100} ⟨001⟩, {102} ⟨201⟩, and {100} ⟨011⟩ within 15° from the ideal orientations and {110} ⟨112⟩, {123} ⟨634⟩, and {112} ⟨111⟩ within 10° from the ideal orientations. The stars indicate one-eighth thickness positions from the surfaces of the 5-cycle processed specimen.

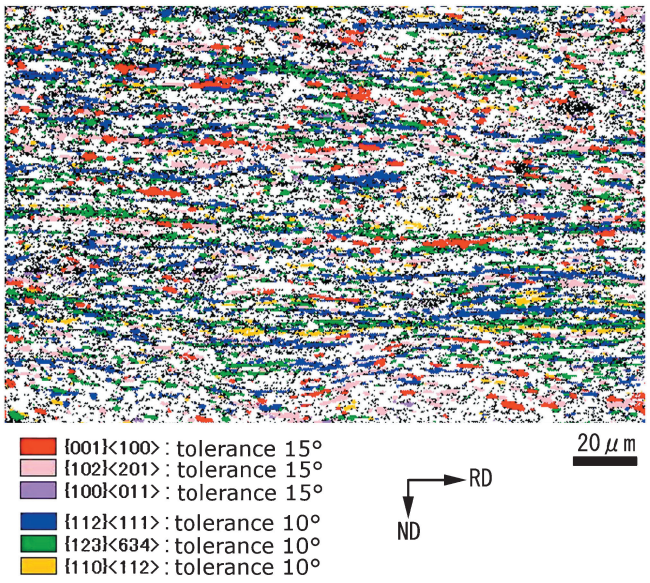

Fig. 6 Magnified deformation structure in the 9-cycle processed specimen.

et al. However, the effect of friction between the specimen and the rolls under lubricated condition in the present study is much smaller than that in the previous study using unlubricated condition.[25,26] In this study, the use of lubricant may have allowed the formation of {123} ⟨634⟩ bands in the one-eighth thickness layers of the 5-cycle processed specimen.

The 5-cycle processed specimen showed the maximum {123} ⟨634⟩ area fraction. However, the area fraction decreased after the 7th cycle. Such a local maximum area fraction of {123} ⟨634⟩ at intermediate ARB cycles around $\varepsilon_{eq} = 4$ was also observed in an ARB experiment using commercial-purity aluminum polycrystal.[27] In this experiment, the volume fraction of {123} ⟨634⟩ measured by an X-ray diffraction method reached its maximum value at a true strain of 3.5 ($\varepsilon_{eq} = 4$). It subsequently decreased with increasing true strain. Alternatively, the volume fraction of {112} ⟨111⟩ gradually increased. After a true strain of 6 has been reached, the volume fractions of {112} ⟨111⟩ and {123} ⟨634⟩ remained relatively constant. The fraction of {112} ⟨111⟩ was higher than that of {123} ⟨634⟩, but this relation is different from the result of the present our study in terms of a β-fiber texture component with the highest area fraction (see Fig. 4). Except for this difference, the previous study[27] and our study indicate that in ARB process {123} ⟨634⟩ is not stable at intermediate cycles around $\varepsilon_{eq} = 4$.

In our study, since the area fraction of {123} ⟨634⟩ decreased after the 7th cycle and conversely the area fraction of {112} ⟨111⟩ increased, {112} ⟨111⟩ was nominated for the crystal orientation resulting from further rotation from {123} ⟨634⟩. In the ARB experiment performed by Heason and Prangnell,[27] the polycrystalline specimen was deformed by ARB without lubrication up to a true strain of 10. {100} ⟨011⟩ orientation produced in the surface layers rotated toward {112} ⟨111⟩, when the {100} ⟨011⟩ surface layer was transferred into the center layer by the next ARB process. The crystal rotation from {100} ⟨011⟩ to {112} ⟨111⟩ was explained by the plane strain compression in the center layer. However, in this study using lubricated condition, {100} ⟨011⟩ could barely be detected during ARB (see Fig. 3). Therefore, it is unlikely that the route in crystal rotation from {100} ⟨011⟩ to {112} ⟨111⟩ is dominant. We concluded that the {123} ⟨634⟩ orientation observed in the 5-cycle processed specimen rotated toward {112} ⟨111⟩ in the 7- and 9-cycle processed specimens under the lubricated condition.

After the 2nd cycle, the area fraction of {100} ⟨001⟩ showed a constant amount of about 6.9%. {100} ⟨001⟩ areas were observed even in the 9-cycle processed specimen

($r = 99.8\%$ and $\varepsilon_{eq} = 7.18$), and the area fraction was 5.8%. The average area fraction of {100} ⟨001⟩ from the 2nd to 9th cycles was 4.8%. We think that {100} ⟨001⟩ areas existing in the deformation structure were subjected to not only grain subdivision but also dynamic recovery; this was because the area fraction of {100} ⟨001⟩ was constant over a wide range of the 2nd to 9th cycles. The stability in the area fraction of {100} ⟨001⟩ may be ascribed to the special slip geometry. In general, dynamic recovery behavior for FCC metals with high stacking fault energy such as aluminum can be explained by cross slip.[28] The cross slip is considered to be a stress relief mechanism in plastic deformation.[29] Cross slip easily occurs when a crystal is deformed along ⟨100⟩, while it rarely occurs when deformed along ⟨111⟩.[30] Assuming that a {100} ⟨001⟩ single crystal is deformed in tension along the *RD* and compression along the *ND*, cross slips occur between two slip system pairs: one pair is a2 and d2, and the other b2 and c2. In highly strained specimens such as the 7- and 9-cycle processed specimens, cross slips occur in abundance in {100} ⟨001⟩ areas, keeping the balance of operations between the two slip system pairs. Therefore, {100} ⟨001⟩ areas can be maintained even in the 9-cycle processed specimen, which had almost the same area fraction as the 2-cycle processed specimen.

The {100} ⟨001⟩ areas were partially adjacent to the {123} ⟨634⟩ or {112} ⟨111⟩ grains after the 9th cycle, as shown in Fig. 6. The {100} ⟨001⟩ single crystal deformed by ARB up to 9 cycles with lubrication was shown to produce both the {100} ⟨001⟩ areas resulting from the cross slips and the {123} ⟨634⟩ and {112} ⟨111⟩ grains formed by the crystal rotations.

5. Conclusions

(1) The weakened texture composed of {123} ⟨634⟩ and {112} ⟨111⟩ developed in the 9-cycle processed specimens ($r = 99.8\%$ and $\varepsilon_{eq} = 7.18$).
(2) After 2 cycles, the area fraction of {100} ⟨001⟩ reaches a steady state. The average area fraction over the 2nd to 9th cycles was 4.8% with a tolerance value of 15° in crystal orientation. The {100} ⟨001⟩ areas existed even in the 9-cycle processed specimen because of the dynamic recovery caused by cross slip.
(3) Under lubricated conditions, the development of {112} ⟨111⟩ after the 7th and 9th cycles was ascribed to further crystal rotation of {123} ⟨634⟩, which achieved the maximum area fraction for the 5-cycle processed specimen. {123} ⟨634⟩ is not stable at intermediate cycles around $\varepsilon_{eq} = 4$ in ARB process.

Acknowledgement

One of the authors (K.K.) acknowledges the financial support provided by the Light Metal Educational Foundation Inc., and N.T. acknowledges the financial support by the Grant-in-Aid for Scientific Research on Innovative Area, “Bulk Nanostructured Metals”, through MEXT, Japan.

REFERENCES

1) R. Z. Valiev, N. A. Krasilnilov and N. K. Tsenev: Mater. Sci. Eng. A **137** (1991) 35–40.
2) R. Z. Abdulov, R. Z. Valiev and N. A. Krasilnikov: J. Mater. Sci. Lett. **9** (1990) 1445–1447.
3) A. P. Zhilyaev, K. Ohishi, T. G. Langdon and T. R. McNelley: Mater. Sci. Eng. A **410–411** (2005) 277–280.
4) M. Furukawa, Y. Kawasaki, Y. Miyahara, Z. Horita and T. G. Langdon: Mater. Sci. Eng. A **410–411** (2005) 194–200.
5) J. Richert and M. Richert: Aluminium **8** (1986) 604–607.
6) M. Richert, Q. Liu and N. Hansen: Mater. Sci. Eng. A **260** (1999) 275–283.
7) Y. Saito, N. Tsuji, H. Utsunomiya, T. Sakai and R. G. Hong: Scr. Mater. **39** (1998) 1221–1227.
8) N. Tsuji, K. Shiotsuki and Y. Saito: Mater. Trans., JIM **40** (1999) 765–771.
9) N. Tsuji, T. Toyoda, Y. Minamino, K. Koizumi, T. Yamane, M. Komatsu and M. Kiritani: Mater. Sci. Eng. A **350** (2003) 108–116.
10) X. Huang, N. Tsuiji, N. Hansen and Y. Miyamoto: Mater. Sci. Eng. A **340** (2003) 265–271.
11) H. Pringazi: Mater. Sci. Eng. A **497** (2008) 132–138.
12) N. Tsuji, Y. Ito, Y. Saito and Y. Miyamoto: Scr. Mater. **47** (2002) 893–899.
13) C. Kwan, Z. Wang and S. Kang: Mater. Sci. Eng. A **480** (2008) 148–159.
14) S. H. Lee, Y. Saito, N. Tsuiji, H. Utsunomiya and T. Sakai: Scr. Mater. **46** (2002) 281–285.
15) B. L. Li, N. Tsuji and N. Kamikawa: Mater. Sci. Eng. A **423** (2006) 331–342.
16) F. J. Humphreys and M. Hatherly: *Recrystallization and related annealing phenomena*, (Pergamon, 1996) p. 354.
17) F. Basson and J. H. Driver: Acta Mater. **48** (2000) 2101–2115.
18) Y. Takatsuji: *Bachelor thesis*, (Kyoto University, 2010) pp. 10–11.
19) P. P. Bhattacharjee, R. K. Ray and N. Tsuji: Acta Mater. **57** (2009) 2166–2179.
20) K. Kashihara and H. Inagaki: Mater. Trans. **48** (2007) 1986–1991.
21) K. Kashihara and T. Shibayanagi: Mater. Trans. **50** (2009) 2192–2200.
22) K. Kashihara, W. Ikushima, Y. Miyajima, D. Terada and N. Tsuji: Proc. 12th Int. Conf. on Aluminum Alloys, Ed. by T. Sato *et al.*, (The Japan Institute of Light Metals, Yokohama, 2010) pp. 2130–2135.
23) J. F. Bishop and R. Hill: Phil. Mag. **42** (1951) 1298–1307.
24) N. Ishida, D. Terada, K. Kashihara and N. Tsuiji: Adv. Mater. Res. **26–28** (2007) 405–408.
25) N. Kamikawa, N. Tsuji, X. Huang and N. Hansen: Acta Mater. **54** (2006) 3055–3066.
26) N. Kamikawa, N. Tsuji, X. Huang and N. Hansen: Mater. Trans. **48** (2007) 1978–1985.
27) C. P. Heason and P. B. Prangnell: Mater. Sci. Forum **408–412** (2002) 733–738.
28) K. Sumino: *Plasticity of Crystals* (in Japanese), Ed. by the Japan Institute of Metals, (Maruzen, Tokyo, 1977) pp. 463–464.
29) S. Miura, J. Takamura and N. Narita: Proc. Int. Conf. on Strength of Metals and Alloys, Ed. by T. Hirone *et al.*, (The Japan Institute of Metals, Sendai, 1968) pp. 555–562.
30) M. Tagami, K. Kashihara, T. Okada and F. Inoko: Mater. Trans. **42** (2001) 2013–2020.